ROYAL SOCIETY OF CHEMISTRY

EDGE ARTICLE

Check for updates

Multivariate sodalite zeolitic imidazolate frameworks: a direct solvent-free synthesis†

Javier López-Cabrelles, [ID] [a] Eugenia Miguel-Casañ,[a] María Esteve-Rochina, [ID] [a] Eduardo Andres-Garcia, [ID] [a] Iñigo J. Vitórica-Yrezábal,[b] Joaquín Calbo [ID] [a] and Guillermo Mínguez Espallargas [ID] *[a]

Different mixed-ligand Zeolitic Imidazolate Frameworks (ZIFs) with sodalite topology, *i.e.* isoreticular to **ZIF-8**, unachievable by conventional synthetic routes, have been prepared using a solvent-free methodology. In particular, the versatility of this method is demonstrated with three different metal centres (Zn, Co and Fe) and binary combinations of three different ligands (2-methylimidazole, 2-ethylimidazole and 2-methylbenzimidazole). One combination of ligands, 2-ethylimidazole and 2-methylbenzimidazole, results in the formation of SOD frameworks for the three metal centres despite this topology not being obtained for the individual ligands. Theoretical calculations confirm that this topology is the lowest in energy upon ligand mixing.

Introduction

Multivariate materials composed of several distinct functional units are attracting interest due to their advanced versatility. Metal–organic frameworks (MOFs)[1–3] offer a unique scenario for such materials due to their intrinsic chemical tunability.[4–6] Zeolitic imidazolate frameworks (ZIFs) are a subclass of MOFs formed by tetracoordinated metal centres and imidazolate linkers, resulting in extended solids with zeolitic topologies.[7,8] The most studied ZIF is arguably **ZIF-8**,[7,8] formed by 2-methylimidazolate (mim) and Zn(II), presenting a sodalite (SOD) topology,[9,10] *i.e.* interconnected porous cages by six and four membered rings with small pore apertures. The SOD topology is not exclusive to **ZIF-8**, and can be obtained through direct synthesis with other metals, such as Co(II),[11] Cd(II),[12] Mg(II),[13] Mn(II),[14] and Fe(II);[15] with substituted imidazole derivatives in the 2-position, such as 2-chloroimidazole,[16] 2-bromoimidazole,[16] 2-nitroimidazole,[17] and 2-carbaldehydeimidazole;[18] or in the 4- and 5-positions, such as benzimidazole.[7,19] Very recently, this number of imidazole derivatives has been further expanded through the use of mechanochemistry.[20]

This versatility in both the metal and the ligand results in the modulation of properties such as the network flexibility, which has shown to be fundamental for key properties, as in catalytic applications,[21,22] and indicates the possibility of fine-tuning the properties through a combination of ligands,[23] as reported in other families of MOFs.[24–29] However, other ligands that would normally form different structures are challenging to be incorporated into the SOD structure of **ZIF-8** through a direct synthesis. In fact, the mixture of such ligands normally induces changes in the topology.[30]

In addition, the inclusion of a second ligand in the SOD topology is of interest to enhance the stability of the framework. In this sense, Friščić, Navrotsky and colleagues have recently suggested a thermodynamic approximation to enhance the ZIFs stability, focussing on the effects of different substituents of the linkers, contrary to the common approach of focussing on the kinetic effects.[20,31,32] Thus, this idea can be extrapolated to obtain thermodynamic stable SOD ZIFs through the combination of several ligands.

Beyond the direct synthesis, alternative synthetic methodologies such as post-synthetic linker-exchange (PSLE) allow materials that are not available by common routes to be obtained.[33] For example, partial exchange of the 2-methylimidazole by 5,6-dimethylbenzimidazole has been achieved through a shell–ligand-exchange-reaction (SLER),[34] whereas anchoring of fluorinated molecules has been possible through thiol-ene click reaction.[35] However, this approach is typically effective only at the surface. Vapour-phase ligand exchange (VPLE) has also been used to incorporate different imidazole derivatives, although it is limited to certain imidazoles, resulting in some cases in a transformation into dense phases.[36] Nevertheless, a major limitation of post-synthetic strategies is the incorporation of additional synthetic steps, which hinders a scalable process and therefore a commercial use.

Herein, we report a direct green synthetic route based on a solvent-free methodology[37,38] to construct mixed-ligand SOD

[a]Instituto de Ciencia Molecular (ICMol), Universidad de Valencia, Paterna 46980, Valencia, Spain. E-mail: guillermo.minguez@uv.es

[b]School of Chemistry, University of Manchester, Oxford Road, Manchester M13 9PL, UK

† Electronic supplementary information (ESI) available. CCDC 2095300 2095301. For ESI and crystallographic data in CIF or other electronic format see DOI: 10.1039/d1sc04779e
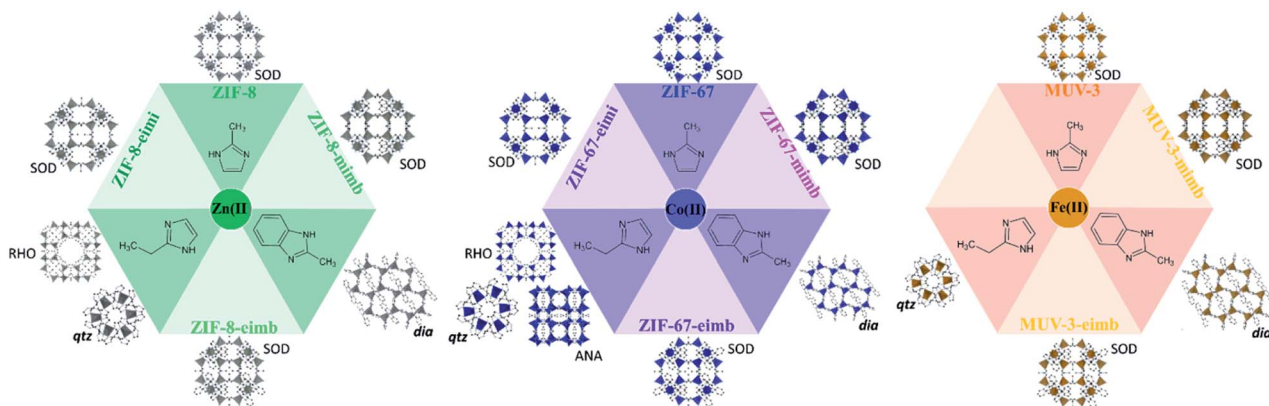
Fig. 1 Scheme of the different achievable crystal structures by solvent–free synthesis combining M(II) and three imidazoles: 2-methylimidazole, 2-ethylimidazole and 2-methylbenzimidazole. The combination of two different imidazoles permits the formation of sodalite materials, in contrast to the dense coordination polymers formed with the pure ligand synthesis.

ZIFs materials unapproachable by pure ligand synthesis. The success of this approach is demonstrated with three different combinations of ligand mixtures and three different metals (Fig. 1). Specifically, we have used different combinations of 2-methylimidazolate (mi), 2-methylbenzimidazolate (mb) and 2-ethylimidazolate (ei), thus using bulkier substituents in the 2-position or in the 4–5-positions (see Fig. 1a). As metal centres, we have explored Zn(II), Co(II) and Fe(II), totalling eight compounds as phase pure crystalline materials, denoted **ZIF-8-mimb**, **ZIF-67-mimb**, **MUV-3-mimb**, **ZIF-8-eimb**, **ZIF-67-eimb**, **MUV-3-eimb**, **ZIF-8-eimi** and **ZIF-67-eimi**, where the initial part of the name indicates the "parent" ZIF with SOD topology (*i.e.* **ZIF-8** for Zn(II), **ZIF-67** for Co(II) and **MUV-3** for Fe(II)) and the second part of the name indicates the mixture of ligands used (mi = 2-methylimidazole, mb = 2-methylbenzimidazole, ei = 2-ethylimidazole).

The pure ligand synthesis using either 2-methylimidazole or 2-ethylimidazole has been previously reported with Zn(II), Co(II) and Fe(II), yielding SOD frameworks in the case of the former (the well-known **ZIF-8**, **ZIF-67** and **MUV-3**); or different polymorphs in the case of the latter, including RHO (**MAF-6**),[8,39] ANA (**MAF-5**)[8,39] and qtz (**MAF-32** and **MUV-7**)[15,39,40] topologies (see Fig. 1 and Section S2.1.2†). In the case of 2-methylbenzimidazole, only the Fe(II) analogue has been previously reported (**MUV-6**),[15] although the Zn(II) and Co(II) analogues can also be prepared with this solvent-free methodology (see Section S2.1.2†).

Results and discussion

A 1 : 1 mixture of the three possible binary combination of ligands results in crystalline solids after 48 h upon reaction with ZnO, cobaltocene or ferrocene at 150 °C. The phase purity and the presence of only one polymorph was determined using X-ray powder diffraction (XRPD), confirming the homogeneity of the crystals obtained during the synthesis and discarding a possible segregation of phases, a common situation when using mixtures of ligands. In eight of the nine possible scenarios, we managed to obtain mixed-ligand structures with a SOD topology

(Fig. 2b–d). Scanning electron micrographs (SEM) show the well-defined morphology of all of the mixed-ZIFs (see Fig. 3b and Section 2.7). In only one situation, when using a mixture of miH and eiH with Fe(II), a qtz framework with only one of the ligands (eiH) was obtained (see Fig. S1†). The presence of two ligands was confirmed by solid-state ^{13}C NMR spectroscopy (Fig. 3a) in the diamagnetic samples (**ZIF-8-mimb**, **ZIF-8-eimb** and **ZIF-8-eimi**). In addition, all the eight mixed-ligand samples were digested in D_2O and deuterated trifluoroacetic acid, and then evaluated by ^{1}H NMR spectroscopy (see Section S2.4†). In all cases, we observed an approximate 2 : 1 ratio in the ligands, with a minor component of the bulkier imidazole derivative. Interestingly, it is possible to slightly modify the final ratio by adjusting the proportion in the synthesis. Nevertheless, we have
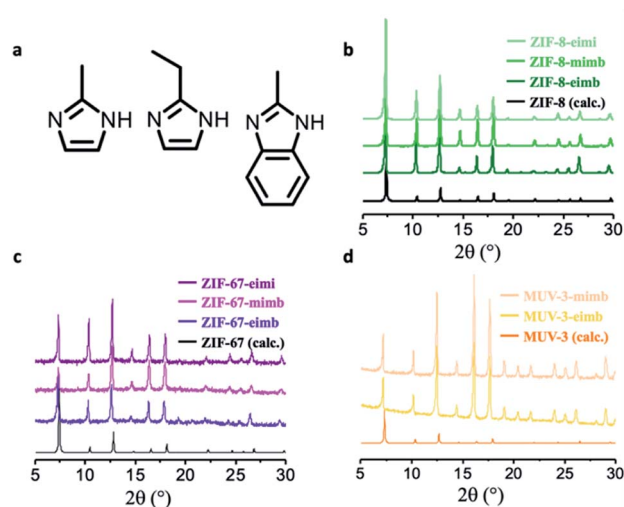

Fig. 2 (a) **ZIF-8**, **ZIF-67** and **MUV-3** are constructed by 2-methylimidazole (mi), which is increased in size with bulkier ligands 2-ethylimidazole (ei) and 2-methylbenzimidazole (mb). (b–d) X-ray powder diffractograms of **ZIF-mimb**, **ZIF-eimb** and **ZIF-eimi** (b, c and d for the different metallic centres, Zn(II), Co(II) and Fe(II), respectively), showing the isoreticularity between them.
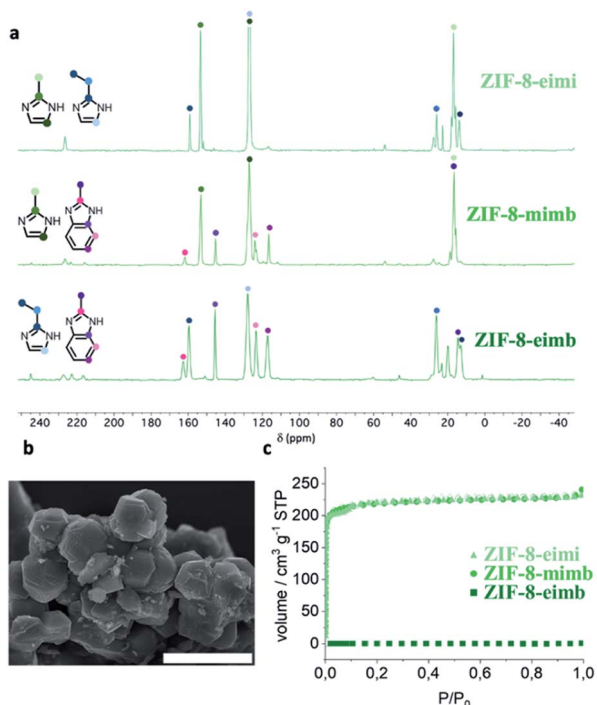
Fig. 3 (a) Solid-state ^{13}C NMR spectra of **ZIF-8-eimi**, **ZIF-8-mimb** and **ZIF-8-eimb**. (b) Scanning electron micrograph of typical **ZIF-8** mixed-ligand compounds. (c) N$_2$ sorption (solid symbols) and desorption (open symbols) of **ZIF-8** mixed-ligand materials at 77 K.

found an upper limit of *ca.* 70% and a lower limit of *ca.* 50% for eiH and miH, respectively.

Importantly, large crystals suitable for X-ray single crystal diffraction were obtained for two compounds, namely **MUV-3-mimb** and **MUV-3-eimb** (see Fig. 4). Structural analysis reveals that both compounds are isoreticular with **MUV-3** (and **ZIF-8** and **ZIF-67**), with similar crystal cell parameters and Fe–N distances (see Table S2†), being slightly larger than **MUV-3**. In addition, the angle θ between the imidazoles and the 4MR plane, as previously defined,[41,42] are similar in the three structures: 74.4°, 75.9° and 77.4° for **MUV-3**,[21] **MUV-3-mimb** and **MUV-3-eimb**, respectively. Interestingly, despite starting with
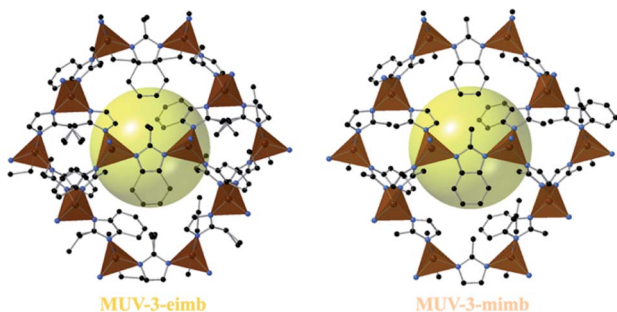

Fig. 4 Crystal structures of **MUV-3-eimb** and **MUV-3-mimb**. Color key: Fe, orange tetrahedra; C, black balls; N, blue balls. Hydrogen atoms are omitted for clarity. The yellow sphere (diameter = 12 Å) is included for better visualization of the void.

a 1 : 1 ratio between the two ligands, their occupancy was included in the refinement, resulting in both cases in a 70 : 30 ratio (mi : mb or ei : mb for **MUV-3-mimb** and **MUV-3-eimb**, respectively), as also found by ^{1}H NMR spectroscopy (see Section S2.4†). Several single crystals were analysed, with similar results for each of them. The confirmed mixed-ligand Fe(II) structures present higher thermal stability (Fig. S12†) compared to **MUV-3**[15] as a result of the incorporation of mb in the structure.

The magnetic behaviour of polycrystalline bulk samples of **MUV-3-mimb**, **MUV-3-eimb**, **ZIF-67-mimb**, **ZIF-67-eimb** and **ZIF-67-eimi** was investigated by SQUID measurements in the range 2–300 K. Variable-temperature direct current (dc) magnetic susceptibility measurements (χ *vs. T*) show an increase upon cooling down until a maximum is reached (Fig. S5 and S6†), indicating the presence of strong antiferromagnetic metal–metal interactions between the M(II), as also observed in **MUV-3**.[15] The maximum in χ is followed by a sharp decrease at lower temperature, which agrees with an antiferromagnetic ordered structure. The presence of a single maximum in the magnetic measurements suggests a single phase transition, related to the presence of only one crystalline phase (Fig. S5 and S6†), discarding the combination of two different phases or pure ligand domains. Moreover, the Néel temperatures (T_N) for the mixed-ligand ZIFs (13.9–17.8 K) are close to the pure ligand SOD materials (17.2–20.6 K), in contrast to the T_N found for dia and qtz topologies (T_N = 32.2 and 35.9 K, respectively, see Section S2.3†).

The porous nature of these mixed-ligand materials has been analysed using N$_2$ sorption measurements, revealing some differences depending on the combination of ligands. Thus, whereas **ZIF-8-mimb** and **ZIF-8-eimi** show BET values of 875 and 845 m^2 g^{-1}, respectively (Fig. 3c), in agreement with previous reports,[43] **ZIF-8-eimb** shows a negligible N$_2$ sorption capacity. On the contrary, for the Co(II) compounds, only **ZIF-67-eimi** presents remarkable porosity, albeit lower than the Zn(II) analogue (BET of 402 m^2 g^{-1}, Fig. S21†), whereas the two mixed-ligand Fe(II) materials present a negligible N$_2$ sorption capacity. This seems to be the result of a smaller window caused by the bulkier ligand combined with a different gate-opening capacity depending on the metal, as previously hypothesized.[22,44] These textural properties are also accompanied by a higher stability towards water, improving their chemical stability and hydrophobicity (see Section S4 in the ESI†).

From the above results, the most counterintuitive outcome is that the mixture of mbH and eiH leads to a material with SOD topology in any of the three metals evaluated. As shown in Fig. 5a, qtz is the most stable topology for the exclusive use of eiH, whereas the most favourable topology for the use of only mbH is the dia topology. In fact, previous attempts to combine mbH with another ligand has resulted in the formation of **JUC-160**[45] and Zn(2mbim)$_{0.28}$(5mbim)$_{1.72}$ (ref. 30) with GIS and ykh topologies, respectively. Thus, we further investigated this from a theoretical point of view. Density functional theory calculations were performed for **ZIF-8**, **ZIF-67** and **MUV-3** in several ligand compositions to assess phase stability (see Section S3 in the ESI† for computational details). Minimum-energy crystal
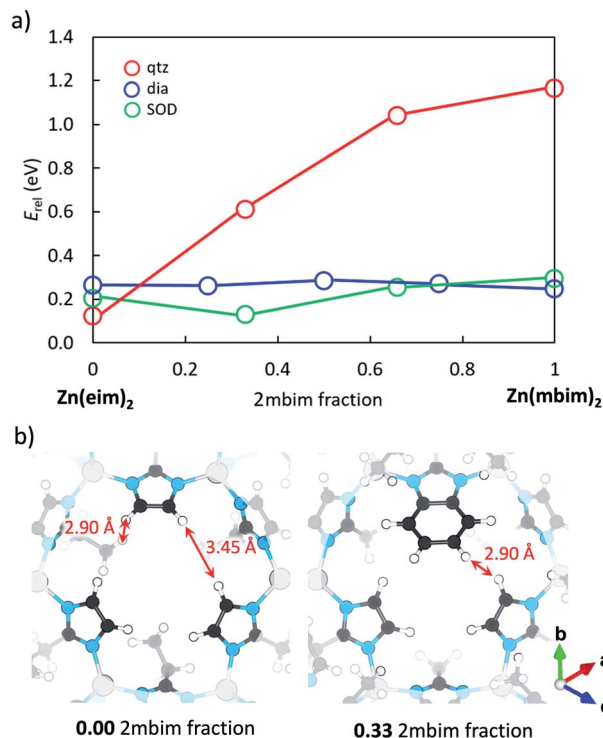
a)

b)

Fig. 5 (a) Phase stability diagram calculated at the PBEsol level for mixed eim:mbim Zn-based **ZIF-8** with respect to the most stable pure-mim **ZIF-8** (the corresponding diagrams for Co and Fe are shown in Fig. S24 and S25†). Lines are drawn to guide the eye. (b) Crystal structure calculated for pure-eim **ZIF-8** (left) and **ZIF-8-eimb** at a 2 : 1 ei : mb composition (right). Relevant H···H distances are indicated.

structures for the pure- and mixed-ligand MOFs at the PBEsol level present cell parameters in good accord with the experimental data (Tables S1, S4 and S5†). Theoretical calculations predict the most stable phases for each pure-ligand ZIF to be SOD for mi, dia for mb, and qtz for ei (Table S4†), in agreement with the polymorphs found experimentally for the zeolitic framework series.[46]

Fig. 5a displays the relative phase energy as a function of the ei : mb ligand mixing ratio in the case of **ZIF-8** (see Fig. S24† for Co-based **ZIF-67** and Fig. S25† for Fe-based **MUV-3**). Upon increasing the mb fraction, the qtz topology rapidly destabilizes up to an energy difference of >1 eV when reaching 100% mb with respect to pure-ei **ZIF-8**. This destabilization can be rationalized by the large steric hindrance promoted through the introduction of bulkier mb ligands with respect to ei in the relatively small qtz unit cell, which suffers a 45% cell expansion in going from pure-ei to pure-mb (Table S4†). In contrast, ligand substitution barely affects phase stability in dia topology, which is computed more stable than qtz for ei:mb ratios of >0.25 (Fig. 5a). Interestingly, the SOD topology, which is not the most stable phase either in pure-ei or pure-mb ZIFs, is predicted the lowest in energy upon ligand mixing, especially at a 2 : 1 ei : mb composition, in the three ZIFs (Fig. 5a, S24 and S25†). A careful inspection of the crystal structure evidences for the 33% mb fraction an effective match of the two ei and one mb ligands at the SOD six-membered ring gate (Fig. 5b), along with additional

ethyl···benzene CH···π interactions between ei and mb (Fig. S28†). On the other hand, the addition of further mb leads to an increased steric hindrance between benzene rings that destabilizes the SOD topology in favour of dia, for 100% mb (Fig. 5a, S24 and S25†).

Conclusions

In summary, the solvent-free synthesis offers a platform with high versatility and applicability, which allows the preparation of multivariate ZIFs, enabling the incorporation of bulkier ligands retaining the sodalite topology. We have demonstrated the versatility of this approach with three different binary combinations of ligands and three different metal centres, resulting in eight novel ZIFs with different response towards N_2 sorption. In this sense, recent studies have shown the importance of the metal centres in lowering the pressure at which the gate opening occurs in **ZIF-8**,[21] but we demonstrate that the use of mixed-ligand frameworks is an alternative approach to modify the physical properties of ZIFs. Theoretical calculations confirm the preference of a SOD topology when using mixture of ligands, which is rationalized by invoking inter-ligand steric hindrance effects. This solvent-free approach allows to design multivariate ZIFs with network complexity, thus opening the door to also combine different metals in the same framework, and paving the way to reach similar complexity in ZIFs as that observed in other promising MOFs.[5] In addition, a further advantage that presents this methodology concerns its facile applicability, involving a solvent-free approach that has proven useful for its processing.[38]

Data availability

All experimental and crystallographic data is available in the ESI.† Crystallographic data for MUV-3-eimb and MUV-3-mimb has been deposited at the CCDC (codes 2095300 and 2095301) and can be obtained from http://www.ccdc.cam.ac.uk/conts/retrieving.html.

Author contributions

J .L. C. synthetized the materials. E. M. C. performed the NMR analysis. E. A. G. conducted the adsorption studies. I .J. V. Y. contributed to solution and refinement of the structures from single crystal data. M. E.-R. and J. C. have performed the theoretical calculations and analyzed the computational data. G. M. E. conceived and designed the experiments. J. L. C. and G. M. E. prepared the manuscript. All authors commented on the manuscript.

Conflicts of interest

There are no conflicts to declare.

Acknowledgements

Notes and references

1 O. M. Yaghi, M. O'Keeffe, N. W. Ockwig, H. K. Chae, M. Eddaoudi and J. Kim, *Nature*, 2003, **423**, 705–714.

2 N. W. Ockwig, O. Delgado-Friedrichs, M. O'Keeffe and O. M. Yaghi, *Acc. Chem. Res.*, 2005, **38**, 176–182.

3 S. Kitagawa, R. Kitaura and S. Noro, *Angew. Chem., Int. Ed.*, 2004, **43**, 2334–2375.

4 H. Deng, C. J. Doonan, H. Furukawa, R. B. Ferreira, J. Towne, C. B. Knobler, B. Wang and O. M. Yaghi, *Science*, 2010, **327**, 846–850.

5 Z. Ji, T. Li and O. M. Yaghi, *Science*, 2020, **369**, 674–680.

6 J. Jiao, W. Gong, X. Wu, S. Yang and Y. Cui, *Coord. Chem. Rev.*, 2019, **385**, 174–190.

7 K. S. Park, Z. Ni, A. P. Côté, J. Y. Choi, R. Huang, F. J. Uribe-Romo, H. K. Chae, M. O'Keeffe and O. M. Yaghi, *Proc. Natl. Acad. Sci. U. S. A.*, 2006, **103**, 10186–10191.

8 X.-C. Huang, Y.-Y. Lin, J.-P. Zhang and X.-M. Chen, *Angew. Chem., Int. Ed.*, 2006, **45**, 1557–1559.

9 Q. Qian, P. A. Asinger, M. J. Lee, G. Han, K. Mizrahi Rodriguez, S. Lin, F. M. Benedetti, A. X. Wu, W. S. Chi and Z. P. Smith, *Chem. Rev.*, 2020, **120**, 8161–8266.

10 L. Yang, S. Qian, X. Wang, X. Cui, B. Chen and H. Xing, *Chem. Soc. Rev.*, 2020, 5359–5406.

11 R. Banerjee, A. Phan, B. Wang, C. Knobler, H. Furukawa, M. O'Keeffe and O. M. Yaghi, *Science*, 2008, **319**, 939–943.

12 Y.-Q. Tian, S.-Y. Yao, D. Gu, K.-H. Cui, D.-W. Guo, G. Zhang, Z.-X. Chen and D.-Y. Zhao, *Chem.–Eur. J.*, 2010, **16**, 1137–1141.

13 S. Horike, K. Kadota, T. Itakura, M. Inukai and S. Kitagawa, *Dalton Trans.*, 2015, **44**, 15107–15110.

14 K. Kadota, E. Sivaniah, S. Bureekaew, S. Kitagawa and S. Horike, *Inorg. Chem.*, 2017, **52334**, 8744–8747.

15 J. López-Cabrelles, J. Romero, G. Abellán, M. Giménez-Marqués, M. Palomino, S. Valencia, F. Rey and G. Mínguez Espallargas, *J. Am. Chem. Soc.*, 2019, **141**, 7173–7180.

16 K. Li, D. H. Olson, J. Seidel, T. J. Emge, H. Gong, H. Zeng and J. Li, *J. Am. Chem. Soc.*, 2009, **131**, 10368–10369.

17 S. Diring, D. O. Wang, C. Kim, M. Kondo, Y. Chen, S. Kitagawa, K. Kamei and S. Furukawa, *Nat. Commun.*, 2013, **4**, 2684.

18 O. M. Yaghi, H. Furukawa, W. Morris, C. J. Doonan and R. Banerjee, *J. Am. Chem. Soc.*, 2008, **130**, 12626–12627.

19 X. HUANG, J. Zhang and X. Chen, *Chin. Sci. Bull.*, 2003, **48**, 1531–1534.

20 N. Novendra, J. M. Marrett, A. D. Katsenis, H. M. Titi, M. Arhangelskis, T. Friščić and A. Navrotsky, *J. Am. Chem. Soc.*, 2020, **142**, 21720–21729.

21 J. G. Vitillo and L. Gagliardi, *Chem. Mater.*, 2021, **33**, 4465–4473.

22 C. M. McGuirk, T. Runčevski, J. Oktawiec, A. Turkiewicz, M. K. Taylor and J. R. Long, *J. Am. Chem. Soc.*, 2018, **140**, 15924–15933.

23 J. A. Thompson, C. R. Blad, N. A. Brunelli, M. E. Lydon, R. P. Lively, C. W. Jones and S. Nair, *Chem. Mater.*, 2012, **24**, 1930–1936.

24 S. Wang, N. Xhaferaj, M. Wahiduzzaman, K. Oyekan, X. Li, K. Wei, B. Zheng, A. Tissot, J. Marrot, W. Shepard, C. Martineau-Corcos, Y. Filinchuk, K. Tan, G. Maurin and C. Serre, *J. Am. Chem. Soc.*, 2019, **141**, 17207–17216.

25 W. J. Newsome, S. Ayad, J. Cordova, E. W. Reinheimer, A. D. Campiglia, J. K. Harper, K. Hanson and F. J. Uribe-Romo, *J. Am. Chem. Soc.*, 2019, **141**, 11298–11303.

26 B. Lerma-Berlanga, C. R. Ganivet, N. Almora-Barrios, S. Tatay, Y. Peng, J. Albero, O. Fabelo, J. González-Platas, H. García, N. M. Padial and C. Martí-Gastaldo, *J. Am. Chem. Soc.*, 2021, **143**, 1798–1806.

27 C.-C. Cao, C.-X. Chen, Z.-W. Wei, Q.-F. Qiu, N.-X. Zhu, Y.-Y. Xiong, J.-J. Jiang, D. Wang and C.-Y. Su, *J. Am. Chem. Soc.*, 2019, **141**, 2589–2593.

28 T. Y. Luo, C. Liu, X. Y. Gan, P. F. Muldoon, N. A. Diemler, J. E. Millstone and N. L. Rosi, *J. Am. Chem. Soc.*, 2019, **141**, 2161–2168.

29 Z. M. Schulte, Y. H. Kwon, Y. Han, C. Liu, L. Li, Y. Yang, A. G. Jarvi, S. Saxena, G. Veser, J. K. Johnson and N. L. Rosi, *Chem. Sci.*, 2020, **11**, 12807–12815.

30 J. Yang, Y. B. Zhang, Q. Liu, C. A. Trickett, E. Gutiérrez-Puebla, M. Á. Monge, H. Cong, A. Aldossary, H. Deng and O. M. Yaghi, *J. Am. Chem. Soc.*, 2017, **139**, 6448–6455.

31 Z. Akimbekov, A. D. Katsenis, G. P. Nagabhushana, G. Ayoub, M. Arhangelskis, A. J. Morris, T. Friščić and A. Navrotsky, *J. Am. Chem. Soc.*, 2017, **139**, 7952–7957.

32 M. Arhangelskis, A. D. Katsenis, N. Novendra, Z. Akimbekov, D. Gandrath, J. M. Marrett, G. Ayoub, A. J. Morris, O. K. Farha, T. Friščić and A. Navrotsky, *Chem. Mater.*, 2019, **31**, 3777–3783.

33 O. Karagiaridi, M. B. Lalonde, W. Bury, A. a. Sarjeant, O. K. Farha and J. T. Hupp, *J. Am. Chem. Soc.*, 2012, **134**, 18790–18796.

34 X. Liu, Y. Li, Y. Ban, Y. Peng, H. Jin, H. Bux, L. Xu, J. Caro and W. Yang, *Chem. Commun.*, 2013, **49**, 9140–9142.

35 Q. Sun, H. He, W. Y. Gao, B. Aguila, L. Wojtas, Z. Dai, J. Li, Y. S. Chen, F. S. Xiao and S. Ma, *Nat. Commun.*, 2016, **7**, 1–7.

36 J. Marreiros, L. Van Dommelen, G. Fleury, R. Oliveira-Silva, T. Stassin, P. Iacomi, S. Furukawa, D. Sakellariou, P. L. Llewellyn, M. Roeffaers and R. Ameloot, *Angew. Chem.*, 2019, **131**, 18642–18646.

37 J. López-Cabrelles, S. Mañas-Valero, I. J. Vitórica-Yrezábal, P. J. Bereciartua, J. A. Rodríguez-Velamazán, J. C. Waerenborgh, B. J. C. Vieira, D. Davidovikj, P. G. Steeneken, H. S. J. van der Zant, G. Mínguez Espallargas and E. Coronado, *Nat. Chem.*, 2018, **10**, 1001–1007.

38 I. Stassen, M. Styles, G. Grenci, H. Van Gorp, W. Vanderlinden, S. De Feyter, P. Falcaro, D. De Vos, P. Vereecken and R. Ameloot, *Nat. Mater.*, 2016, **15**, 304–310.

39 B. N. Bhadra, P. W. Seo, N. A. Khan and S. H. Jhung, *Inorg. Chem.*, 2016, **55**, 11362–11371.

40 P. J. Beldon, L. Fábián, R. S. Stein, A. Thirumurugan, A. K. Cheetham and T. Friščić, *Angew. Chem., Int. Ed.*, 2010, **49**, 9640–9643.

41 C. L. Hobday, T. D. Bennett, D. Fairen-Jimenez, A. J. Graham, C. A. Morrison, D. R. Allan, T. Düren and S. A. Moggach, *J. Am. Chem. Soc.*, 2018, **140**, 382–387.

42 C. L. Hobday, C. H. Woodall, M. J. Lennox, M. Frost, K. Kamenev, T. Düren, C. A. Morrison and S. A. Moggach, *Nat. Commun.*, 2018, **9**, 1–9.

43 H. M. Titi, J. L. Do, A. J. Howarth, K. Nagapudi and T. Friščić, *Chem. Sci.*, 2020, **11**, 7578–7584.

44 E. Andres-Garcia, J. López-Cabrelles, L. Oar-Arteta, B. Roldan-Martinez, M. Cano-Padilla, J. Gascon, G. Mínguez Espallargas and F. Kapteijn, *Chem. Eng. J.*, 2019, **371**, 848–856.

45 L. Huang, M. Xue, Q. Song, S. Chen, Y. Pan and S. Qiu, *Inorg. Chem. Commun.*, 2014, **46**, 9–12.

46 Note that RHO and ANA topologies are not considered as (i) they are only detected experimentally for pure-eim ZIFs of Zn(II) and Co(II), (ii) they are found higher in energy compared to qtz polymorph (see ref. 31), and (iii) they are highly computationally demanding.